THE JOURNAL OF PHYSICAL CHEMISTRY C

Article

pubs.acs.org/JPCC

Shining a Light on *s*-Triazine-Based Polymers

Cristina Butchosa,[†] Tom O. McDonald,[‡] Andrew I. Cooper,[‡] Dave J. Adams,*[,‡] and Martijn A. Zwijnenburg*[,†]

[†]Department of Chemistry, University College London, 20 Gordon Street, London WC1H 0AJ, United Kingdom

[‡]Department of Chemistry and Centre for Materials Discovery, University of Liverpool, Crown Street, Liverpool L69 7ZD, United Kingdom

Supporting Information

ABSTRACT: The strong interplay between the structure and optical properties of conjugated *s*-triazine-based framework (CTF) materials is explored in a combined experimental and computational study. The experimental absorption and fluorescence spectra of the CTF-1 material, a polymer obtained through the trimerization of 1,4-dicyanobenzene, are compared with the results of time-dependent density functional theory and approximate coupled cluster theory (CC2) calculations on cluster models of the polymer. To help explain the polymer data, we compare its optical properties with those measured and predicted for the 2,4,6-triphenyl-1,3,5-triazine model compound. Our analysis shows that CTFs, in line with experimental diffraction data, are likely to be layered materials based around flat hexagonal-like sheets and suggests that the long-wavelength part of the CTF-1 absorption spectrum displays a pronounced effect of stacking. Red-shifted peaks in the absorption spectrum appear that are absent for an isolated sheet. We also show that the experimentally observed strong fluorescence of CTF-1 and other CTF materials is further evidence of the presence of rings in the layers, as structures without rings are predicted to have extremely long excited state lifetimes and hence would display negligible fluorescence intensities. Finally, subtle differences between the experimental absorption spectra of CTF-1 samples prepared using different synthesis routes are shown to potentially arise from different relative arrangements of stacked layers.

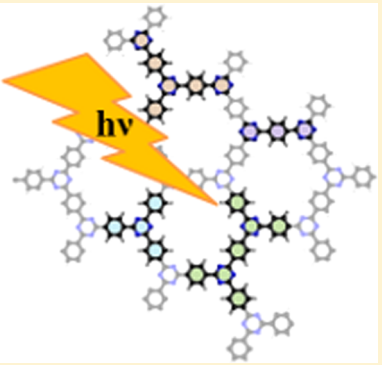

INTRODUCTION

Conjugated triazine-based frameworks (CTFs),[1−7] polymers based around *s*-triazine (1,3,5-triazine) cores, form a fascinating group of materials between the world of inorganic carbon nitride (CN_x) polymers[8−10] and organic conjugated microporous polymers (CMPs).[6,11−13] These CTF polymers consist of *s*-triazine cores connected to each other by three conjugated organic struts and can be formed by the trimerization of organic dinitriles. CTFs have been prepared with a wide-range of struts, the simplest of which is 1,4-dicyanobenzene. (See Scheme 1A.)[1−5] The resulting materials are typically microporous, display fluorescence, generally have very high surface areas, and have been shown to act as heterogeneous catalysts for base-catalyzed reactions.[1−5,14] The properties of the CTFs can be varied by changing the length and chemical characteristics of the strut. The original synthesis routes for CTFs involved high-temperature ionothermal synthesis in molten $ZnCl_2$,[2,4,15] but more recently similar CTFs have been prepared in organic solvents using trifluoromethanesulfonic acid as a catalyst.[5,16]

On the basis of the three-fold nature of the *s*-triazine cores and an analysis of the very broad X-ray diffraction patterns for CTFs, it has been suggested that the average structure of these materials might resemble stacks of hexagonal sheets, not unlike graphite.[2] It is difficult, however, to say much more about the structure by experiment alone due to the poorly crystalline nature of the prepared materials. There is also a clear effect of the preparation method that goes beyond the average structure; the materials prepared in ionothermal synthesis are black,[2] while those made using trifluoromethanesulfonic acid as a catalyst range in color from pale-yellow to brown,[5] although both materials display similarly broad X-ray diffraction patterns.

Here we build upon our recent work on pyrene-based CMPs[17,18] to access structural information from the CTFs' UV−vis absorption and fluorescence spectra through a comparison with theoretical calculations on cluster models of possible chromophores. We focus our work here on the CTF obtained through the cyclotrimerization of 1,4-dicyanobenzene (CTF-1,[2] ionothermal synthesis; P1,[5] trifluoromethanesulfonic acid catalyzed; P1M,[5] trifluoromethanesulfonic acid catalyzed and heated using a microwave rather than by conventional means). We first study 2,4,6-triphenyl-1,3,5-triazine (TP_3, see Scheme 1B) as a well-defined model compound that resembles a key part of the 1,4-dicyanobenzene CTF structure and then expand our work to the chromophores possibly present in the 1,4-dicyanobenzene CTF. Following this procedure, we show that stacking is likely a key contributor to CTF absorption spectra and that the fact that 1,4-dicyanobenzene CTF materials experimentally display fluorescence tells a lot about the materials structure.

Received: December 3, 2013
Revised: December 23, 2013
Published: January 30, 2014

   dx.doi.org/10.1021/jp411854f | *J. Phys. Chem. C* 2014, 118, 4314−4324

Scheme 1. (A) Idealized Structure of the 1,4-Dicyanobenzene CTF and (B) Structure of Triphenyl-*s*-triazine (TP_3)

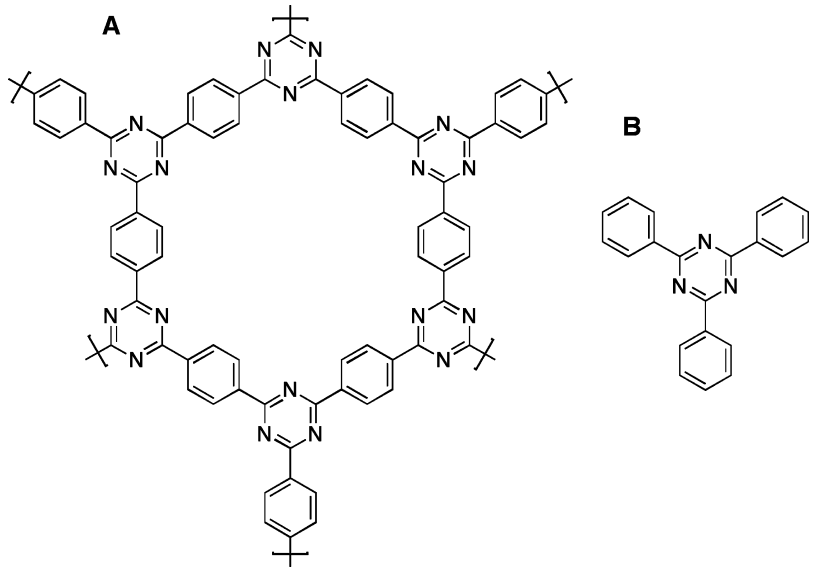

EXPERIMENTAL SECTION

Materials. All reagents and solvents were purchased from Sigma Aldrich. Solution ^{1}H NMR and ^{13}C NMR spectra were collected on a Bruker Avance 400 MHz NMR spectrometer with Samplejet Autosampling robot.

Synthesis of TP_3. TP_3 was synthesized using a Chemspeed Swing robotic platform under ambient conditions. Trifluoromethanesulfonic acid (98%) (TFMS) (3600 mg, 24 mmol) and anhydrous chloroform (4 mL) were charged into a 40 mL glass vial with PTFE-silicone septa with magnetic stirring. A solution of benzonitrile (412 mg, 4 mmol) in anhydrous chloroform (24 mL) was then added to the TFMS solution at 1 mL/min. The reaction was left to proceed for 48 h before 8 mL of 15% aqueous ammonia solution was added to neutralize the acid. The reaction was left stirring for 3 h after the addition of the ammonia solution. The mixture was then poured into 110 mL of methanol resulting in a turbid white suspension. The crude product was obtained by filtration (Whatman PTFE filter tube (5 μm)) before being purified by recrystallization from a chloroform/ethanol mixture (1:1) to give white crystals. Yield 278 mg (67%). ^{1}H NMR (400 MHz, $CDCl_3$) 8.80−8.78 (m, 6H), 7.64−7.56 (m, 9H) ppm. ^{13}C NMR (100 MHz, $CDCl_3$) 171.68, 136.26, 132.53, 128.99, 128.66 ppm. These values agree with those found in the literature.[19] Mass spectroscopy analysis (using positive polarity, Cl chemical ionization and in methane) found m/z 310.1337 corresponding to $(M+H)^+$. The melting point of TP_3 as measured by differential scanning calorimetery (Q2000 DSC (TA Instruments) using a temperature ramp of 2 °C/min) was found to be 236 °C, in agreement with the literature value of 235−237 °C.[19,20]

Optical Characterization. Solution measurements for TP_3 were obtained at 0.0002 mg/mL in dichloromethane. Samples for spectroscopy on solid-state TP_3 powders were obtained by grinding the sample before adding the sample to a quartz powder holder. Also, a film-like solid sample was prepared: TP_3 (2 mg) was dissolved in chloroform (1 mL); this solution was then added to a quartz cuvette held at an angle and left overnight to evaporate. The resulting precipitate on the inside of the cuvette provided a range of film thicknesses for analysis (thickest at the bottom of the cuvette). Data for the P1M polymer were taken from our previous work.[5]

UV−vis spectra were obtained using a Shimadzu UV-2550 UV−vis spectrophotometer running the UVProbe software, version 2.34. All spectra were measured from 200−800 nm, with scan speed set to fast and using a slit width of 5 nm. Film and solution samples were measured in a quartz cuvette as a transmission measurement. Solid powdered samples were analyzed using the ISR-2200 integrating sphere attachment with a quartz solid sample holder as diffuse reflection measurement.

Emission and excitation spectra were obtained using a Shimadzu RF-5301PC spectrofluorophotometer running RFPC software, version 2.04. Spectra were obtained using a high scan speed and with sensitivity set to high. Slit widths were adjusted so as to maximize the signal-to-noise ratio for each sample. Solution samples were analyzed in a quartz cuvette with the standard cell holder attachment. Film-like samples were analyzed adhered to the wall of a quartz cuvette placed in the solid (powder) holder attachment. Powder samples were analyzed in a quartz solid sample holder held in the solid (powder) sample holder attachment. Data was exported to Microsoft Excel for further processing.

Computational Methods. To computationally study the optical properties of triazine-based polymers, we employed a six-step approach. First, for large oligomers, conformational sampling was performed to find low-energy conformers. Second, the singlet ground state (S_0) of the low(est)-energy conformers was optimized using density functional theory (DFT). For selected oligomers, the effect of the solvent has also been considered. Third, where possible, harmonic frequency calculations were performed (using the same DFT setup) to verify that the structures obtained in the S_0 optimization are proper ground-state minima. Fourth, the vertical excitation spectra of the oligomers were calculated using both time-dependent-DFT[21,22] (TD-DFT) and the approximate coupled-cluster singles-and-doubles method (CC2).[23] Fifth, the first exited-state (S_1) of each oligomer was relaxed to obtain its excited-state minimum energy geometry and a prediction of the fluorescence energy using TD-DFT. Finally, for selected oligomers, numerical frequency

dx.doi.org/10.1021/jp411854f | J. Phys. Chem. C 2014, 118, 4314−4324

calculations were performed on the excited-state minima to verify that these correspond to proper minima on the TD-DFT S_1 energy surface.

For the initial conformational search, the OPLS-2005 force field[24] and the low-mode sampling[25] algorithm, as implemented in Macromodel 9.9,[26] were employed. We typically used a combination of 10 000 Monte Carlo search steps and minimum and maximum low-mode move distances of 3 and 6 Å, respectively. All structures located within an energy window of 100 kJ/mol relative to the lowest energy conformer were saved.

Two different hybrid exchange-correlation (XC) functionals were employed in the DFT and TD-DFT calculations: B3LYP[27] and CAM-B3LYP.[28] CAM-B3LYP is a range-separated XC-functional with (relative to B3LYP) a higher percentage of Hartree−Fock exchange at long distances, and as a result the asymptotic behavior of the CAM-B3LYP XC-potential (the derivative of the XC-functional with respect to the distance r) will be closer to the formal $1/r$ dependence of the exact functional. This can be of great importance in the case of conjugated polymers.[28] In all TD-DFT calculations, the Tamm−Dancoff approximation was used, which fixes among other things problems with triplet instabilities present in full TD-DFT.[29,30] For B3LYP calculations, generally the double-ζ DZP basis set[31] was used while for the CAM-B3LYP calculations we typically employed the 6-31G** basis set.[32] A limited number of calculations with other basis-sets such as def2-SV(P)[31] and def2-TZVPP[33] were performed for selected systems to check the effect of the basis set size on the results. The COSMO solvent model was used with the dichloromethane (DCM) relative permittivity of 9.1 to include the effect of solvent in the S_0 optimization and vertical excitation energy.[34,35]

Lifetimes of excited states were calculated using Einstein's equation for spontaneous emission and oscillator strengths calculated in the dipole-length gauge. Use of other gauges (i.e., dipole-velocity or mixed gauge) results in slightly different excited-state lifetimes but does not significantly change the comparison between different cluster models and different states. All spectra shown employed a Gaussian broadening of 0.05 eV and were normalized such that the most prominent peak has a normalized intensity of 1.

The CC2 calculations were performed using both the frozen-core approximation and the resolution-of-the-identity (RI-CC2) approximation to the electron repulsion integrals. The majority of RI-CC2 calculations, for reasons of computational tractability, employed the small def2-SV(P) split-valence basis, but for single points on the smallest oligomers the larger triple-ζ def2-TZVPP basis set was also employed.

All B3LYP and RI-CC2 calculations were performed with the Turbomole 6.4 code.[36,37] The CAM-B3LYP calculations used the NWChem 6.0 code,[38] except in the case of the CAM-B3LYP S_1 relaxations, which were performed with GAMESS-(US) code[39] (version 1 October 2010 R1).

RESULTS AND DISCUSSION

First, we will compare experimental spectra with predictions for molecular TP_3, exploiting the fact that we know the structure of TP_3 and that thus any discrepancies between theory and experiment must arise from issues with the theoretical description. Then, having convinced ourselves of the ability of TD-DFT to correctly predict the optical properties of triazine-based materials, we use a combination of theory and experimental spectroscopy to elucidate possible chromophores in CTFs.

Triphenyl-*s*-triazine: TP_3. The absorption spectrum of TP_3 has been obtained experimentally in three different forms: as a crystalline powder, in a solution of DCM, and as a thin film precipitated as a residue on the wall of the cuvette. As can be seen in Figure 1, the absorption spectrum changes quite

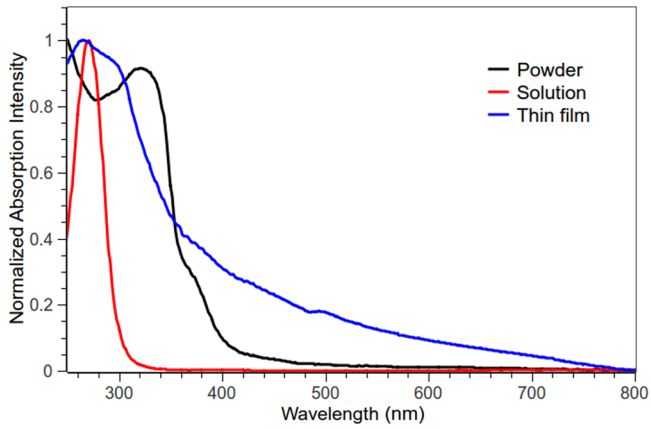

Figure 1. Experimental absorption spectra of triphenyl-*s*-triazine (TP_3) obtained in three different forms: crystalline powder (black), DCM solution (red), and a thin film precipitated as a residue on the wall of the cuvette (blue).

considerably when going from solution (measured in transmission mode) to powder (measured in diffuse reflection mode). The spectra overall broaden and the top of the first peak in the absorption is significantly red-shifted (by ∼60 nm, ∼0.75 eV). Measurement of the absorption spectrum of the thin-film TP_3 precipitate shows a much smaller red shift relative to the solution than that of the powder measured in diffuse reflection mode (∼10 nm, ∼0.2 eV), although there is also considerable peak broadening. These spectral differences between solution and solid-state data probably arise from a combination of true electronic and vibrational differences between TP_3 in solution and the solid state and, especially in the case of the powder sample, from physical effects related to scattering and reflections of light, absent in transmission solution experiments. In line with reports in the literature,[40,41] we found TP_3 to be effectively nonfluorescent (in agreement with the results of our calculations discussed later).

Calculations to predict the absorption spectra of TP_3 were performed at different levels of theory. As can be seen in Figure 2, the TD-B3LYP/DZP calculated spectrum is in good agreement with the experimental solution spectrum. Both the effect of using a larger basis set (def2-TZVPP instead of DZP) and that of including the effect of solvation via a solvation model (COSMO with the DCM dielectric constant of 9.1) on the predicted spectrum are small. For example, a calculation using COSMO displays a red shift of the main absorption peak of ∼4 nm relative to the gas-phase calculation (B3LYP/def2-TZVPP max. absorption is 4.61 eV, 269 nm and B3LYP/def2-TZVPP with DCM max. absorption is 4.54 eV, 273 nm). Calculations using the long-range corrected CAM-B3LYP XC-functional yield a qualitatively similar spectrum as obtained in experiment and with B3LYP, but in line with previous experience with this functional,[28] the spectrum is blue-shifted by 28 nm (0.54 eV) relative to the experimental solution data. Finally, CC2/def2-TZVPP single-point calculations on the B3LYP optimized ground-state

dx.doi.org/10.1021/jp411854f | J. Phys. Chem. C 2014, 118, 4314−4324

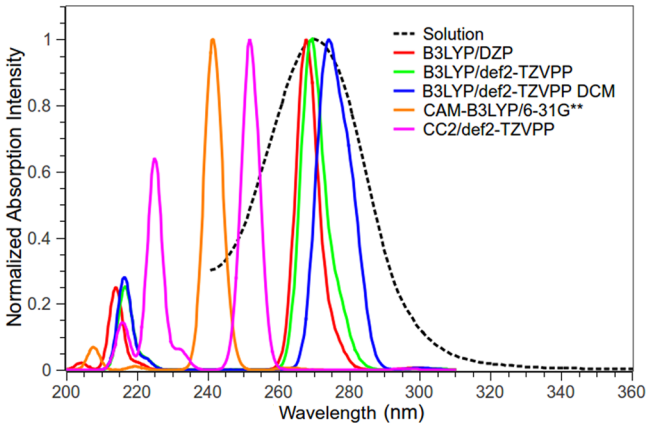

Figure 2. Absorption spectra of triphenyl-*s*-triazine (TP_3). Continuous lines correspond to the result of TD-DFT and CC2 calculations. The black interrupted line is the experimental absorption spectrum of triphenyl-*s*-triazine (TP_3) in a DCM solution.

geometry of TP_3 give very similar excitation energies as TD-B3LYP. (CC2 calculations with the smaller split-valence def2-SV(P) basis set lie ~0.15 eV higher in energy.)

As can be seen in Table 1, there are only some rather subtle differences in the ordering of the different excitations between

Table 1. Vertical Singlet Excitation Energies (EEs) of Triphenyl-*s*-triazine (TP_3) Calculated with Different Theoretical Methods[a]

B3LYP/DZP (Turbomole) (C_{2v})		B3LYP/-def2-TZVPP (Turbomole) (C_{2v})		B3LYP/def2-TZVPP in DCM (Turbomole)	CAM--B3LY-P/6-31G** (NWchem) (C_{2v})		B3LYP/DZ-P //CC2/S-V(P) (Turbomole) (C_{2v})	
irrep	EE	irrep	EE	EE	irrep	EE	irrep	EE
a2	4.05	a2	4.01	4.04	a2	4.56	a2	4.27
b1	4.10	b1	4.08	4.06	a2	4.65	a2	4.34
b2	4.13	b2	4.09	4.11	b1	4.65	b2	4.34
a2	4.13	a2	4.09	4.11	b1	4.71	b2	4.36
b2	4.15	b2	4.11	4.13	b2	4.85	b1	4.62
a1	4.46	a1	4.43	4.40	b2	5.09	b1	4.84
b1	4.46	b1	4.43	4.40	a1	5.09	a1	4.84
b1	4.51	a1	4.49	4.43	a1	5.14	b1	4.96
a1	4.51	b1	4.49	4.43	b2	5.14	a1	5.09
a1	4.51	a1	4.50	4.45	b2	5.18	b1	5.09
b1	4.54	b1	4.54	4.49	a1	5.41	a1	5.29
a1	4.56	a1	4.55	4.50	a1	5.65	a1	5.58

[a]Results reported for the C_{2v} subgroup of the true D_{3h} symmetry because the CC2 and TD-CAM-B3LYP implementations used cannot handle non-Abelian point-groups. TD-B3LYP/DCM calculations performed in C_1 for similar reasons.

CC2/def2-TZVPP and TD-B3LYP, which probably find their origin in the small energy differences between the different excited states. The strong peak in Figure 2 does not correspond to the lowest singlet excitation S_1, which is predicted to have a relatively very low intensity and gives rise to the shoulder at ~300 nm, but rather S_6, S_9, S_{10}, and S_{12}. These higher intensity excitations have $\pi \rightarrow \pi^*$ character, while S_1 has $n \rightarrow \pi^*$ character (i.e., involves the lone pairs on the nitrogen atoms).

To explore the possibility of electronic effects contributing to the considerable red shift of the first main absorption peak for the powder sample, we performed TD-DFT calculations on a series of stacked TP_3 molecules. More specifically, we calculate the vertical excitation spectra of a series of stacks of TP_3 molecules, the geometry of which was based on the TP_3 crystal structure reported by Lindeman et al.[42] It is of interest to note here that in contrast with the gas-phase structure obtained in calculations, the TP_3 molecules in the crystal structure are not planar and the phenyl groups come out of the triazine plane. (See Figure 3.) This distorted geometry of TP_3 in the crystal

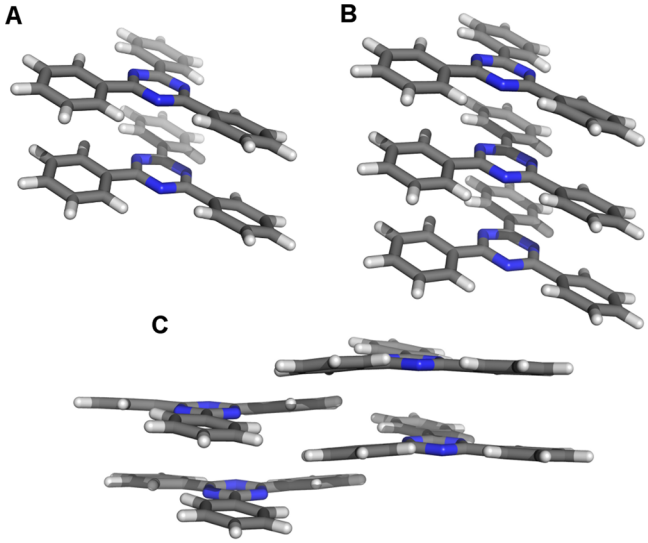

Figure 3. Geometries of some of the stacks of TP_3 molecules used in the study: CS2 (A), CS3 (B), and CSL4 (C, a lateral stack of two CS2).

structure (TP_3 CS1) in itself does not lead to significant changes in the TP_3 absorption spectrum, only a minor blue shift of ~10 nm.

We cut stacks of up to four TP_3 molecules for the crystal structure (CS2, CS3, and CS4). The TD-DFT calculations for CS3 and CS4 are computationally rather expensive (e.g., 200 roots have been calculated in the case of CS3 to obtain the spectra shown in Figure 4), and thus the def2-SV(P) split-valence basis set was used to reduce the cost of these calculations. Use of this smaller basis set leads to a change in the lowest excitation energy relative to the def2-TZVP result of only 0.03 and 0.06 eV for the CS1 molecule and CS2 stack, respectively (Table 2). TD-B3LYP spectra for the different stacks shown in Figure 4 show that stacking leads to the formation of a new red-shifted shoulder at 290 nm and a blue shift of the main absorption peak to 250 nm. Moreover, Figure 4 also shows that with every molecule added to the stack the shoulder further red shifts and grows in intensity. Including stacks laterally (CSL4, see Figure 3) only leads to relatively minor further changes to the predicted spectra at long wavelength. (See Figure S1 in the section ESI-1 of the Supporting Information.)

The CC2/def2-SV(P) calculations in Table 2 display a similar red shift for the lowest excitation energy of the stacks as TD-B3LYP. TD-CAM-B3LYP, in contrast, finds only a marginal red shift of the lowest excitation energy of the stacks and no appreciable red shift of the spectrum. (See section ESI-2 of the Supporting Information for a discussion about the issues with CAM-B3LYP.) CC2/def2-SV(P) spectra calculations (i.e., including calculation of the oscillator strengths for all excitations) for the low-symmetry CS stacks were not tractable on resources available to us. To get an idea of the effect on stacking on the shape of spectra when calculated with CC2, we

dx.doi.org/10.1021/jp411854f | J. Phys. Chem. C 2014, 118, 4314−4324

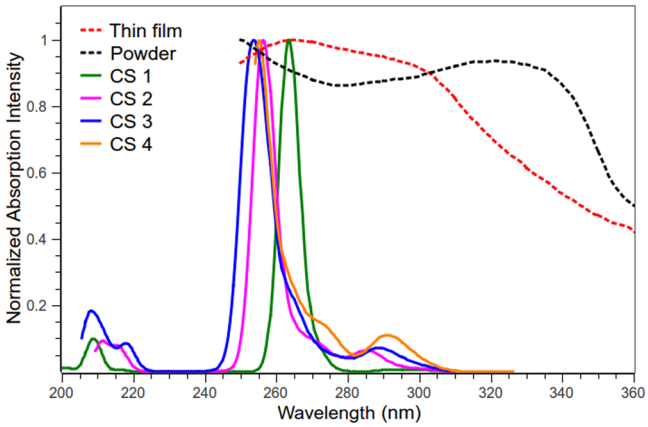

Figure 4. Absorption spectra of different stacks of TP_3 molecules compared with those measured experimentally. Continuous lines correspond to the calculated TD-B3LYP/def2-SV(P) spectra of a different number of stacked monomers cut from a TP_3 crystal.[42] The interrupted lines are the experimental UV absorption for TP_3 as a powder (black) and as a thin film (red).

instead performed a calculation on a stack of two TP_3 molecules in their gas-phase minimum energy structure (GS2). The as-such obtained spectra for GS1 and GS2 (see Figure S2 in section ESI-1 of the Supporting Information for TD-B3LYP and CC2 examples) are very similar to their CS1 and CS2 counterparts. Most importantly, just as for TD-B3LYP, the CC2 spectra show a red shift and an increase in the intensity of the long wavelength shoulder.

On the basis of the TD-B3LYP and CC2 calculations, we believe that the experimentally observed differences between the solution and powder absorption spectra find their origin in the stacking of TP_3 in the solid-state. In this scenario, the peak at 330 nm is not a red-shifted version of the main peak observed in the solution spectrum at 270 nm but rather a new peak and the experimental realization of the red-shifted shoulder observed in the calculations. The main peak itself shifts to the blue in both experiment (from 270 nm to a wavelength smaller than 260 nm) and in the calculations (from 270 to 250 nm). The "halfway" absorption spectrum of the thin-film sample can then also be understood as arising from a disordered structure with only limited stacking.

TP_3 thus seems to display both J- (red-shifted shoulder) and H-aggregate[43−46] (main peak) like behavior in the solid-state. The microscopic basis for this behavior appears to be complicated. In all methods (i.e., both TD-DFT and RI-CC2), the transition dipole moments of the highest oscillator strength excitations (in the gas-phase geometry instead of the CS geometry, as the former is more simple to analyze due to its planar nature) are aligned perpendicular to the stacking axis and hence based on Kasha's exciton model[45] could explain the H-aggregate behavior of the main peak. However, there are also some less strong and lower energy excitations that have transition dipole moments aligned parallel to the stacking axis and lie in a head-to-tail arrangement in the crystal. It is most likely that these latter excitations, again inline with Kasha's exciton model,[45] lead to the observed red shift in the spectra and the J-aggregate-like behavior, resulting in the appearance of the red-shifted shoulder.

Finally, we predicted the fluorescence energy of TP_3 by geometry optimizing its lowest singlet S_1 excited state. We find that TP_3 would have a fluorescence peak at 466 nm (2.66 eV, TD-B3LYP) but that it also predicted to have an extremely long lifetime (0.08 s) at the S_1 minimum energy geometry, as calculated using Einstein's equation for spontaneous emission. A CC2/def2-SV(P) excited-state optimization of S1 finds a similar minima (2.73 eV, 454 nm) reinforcing our trust in the TD-B3LYP result. The lack of experimental observation of fluorescence of TP_3 thus probably finds its origin in this long lifetime, which makes dark de-excitation pathways (i.e., internal conversion) competitive with fluorescence.

1,4-Dicyanobenzene CTF. We will now discuss the optical properties of triazine-based polymers. Figure 5 shows the powder absorption and fluorescence spectra of the P1 and P1M polymers, obtained by polymerizing 1,4-dicyanobenzene (data taken from our previous work[5]). P1 and P1M show a similar two-peak absorption spectrum as TP3, but compared with the latter, the P1 and P1M absorption spectra are red-shifted by ∼50 nm (∼0.4 eV). The P1 and P1M absorption spectra, just as the powder and thin-film TP_3 spectra, also display a long wavelength tail that probably finds it origin in physical light scattering by the polymer particles. We observed similar scattering at long wavelength previously in our work on pyrene CMPs.[18] Finally, the P1 and P1M polymer are clearly fluorescent, in contrast with TP_3, with a fluorescence peak maxima at ∼500 nm (2.5 eV).

To understand the photophysics and photochemistry of the 1,4-dicyanobenzene CTF in general and the P1M sample in particular, we performed TD-DFT calculations on a series of cluster models (oligomers) representing possible structural elements (chromophores). Following our previous work on pyrene-based polymers,[18] these cluster models include both dendrimer-like structures (Figure 6) and rings (i.e., closed loops, Figure 7).

Table 2. Vertical Singlet Excitation Energies Calculated with Different Theoretical Methods for a Single TP_3 Monomer (CS1) and for a Stacked Pair (CS2)[a]

CS1			CS2		
B3LYP/def2-SV(P)[B3LYP/DZP]	CAM-B3LYP/6-31G**	CC2/def2-SV(P)	B3LYP/def2-SV(P)[DZP]	CAM-B3LYP/6-31G**	CC2/def2-SV(P)
4.13 [4.15]	4.62	4.39	4.09 [4.09]	4.61	4.34
4.15 [4.16]	4.71	4.45	4.11 [4.12]	4.61	4.35
4.21 [4.24]	4.73	4.47	4.11 [4.14]	4.70	4.39
4.24 [4.26]	4.77	4.50	4.12 [4.14]	4.71	4.39
4.25 [4.27]	4.89	4.73	4.19 [4.21]	4.72	4.41
4.51 [4.52]	5.11	4.94	4.20 [4.22]	4.72	4.42
4.53 [4.53]	5.12	4.95	4.20 [4.23]	4.77	4.44
4.54 [4.55]	5.17	5.06	4.21 [4.23]	4.79	4.45

[a]These structures where cut from the TP_3 crystal structure obtained by Lindeman et al.[42]

dx.doi.org/10.1021/jp411854f | J. Phys. Chem. C 2014, 118, 4314−4324

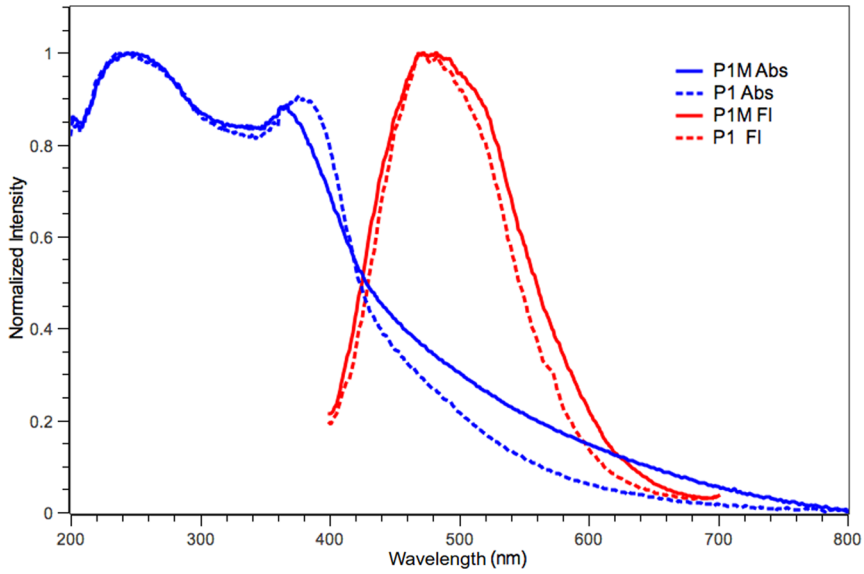

Figure 5. Experimental absorption (blue) and fluorescence (red) spectra of the P1 (interrupted lines) and P1M (uninterrupted lines) polymers.[5]

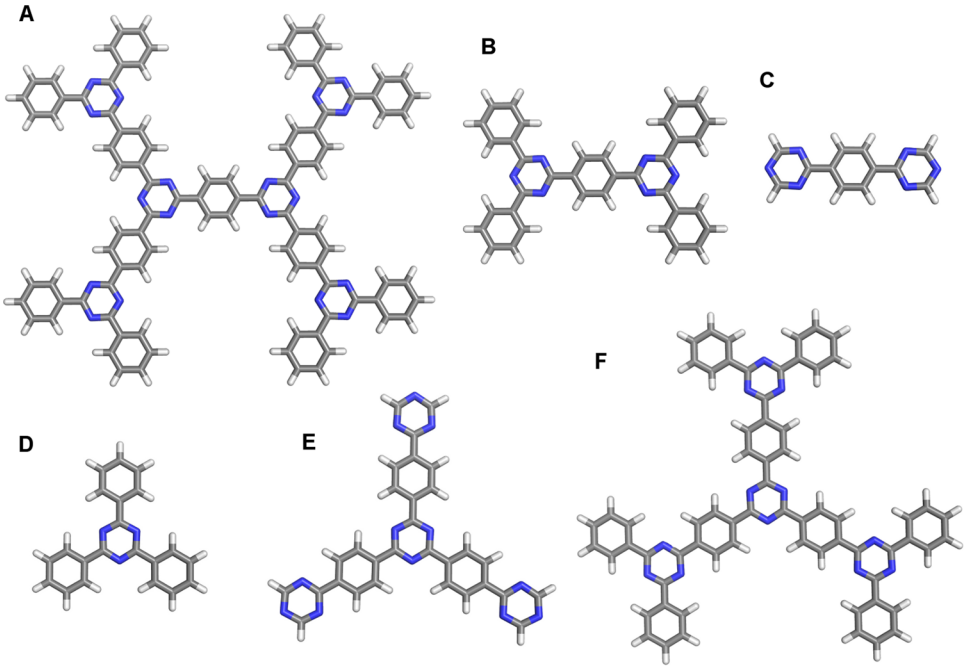

Figure 6. Dendrimer models of the 1,4-Dicyanobenzene CTF.[5] The nomenclature defines the ring in the center of the dendrimer (where T stands for triazine and P stands for phenyl) and then the number of concentrically linked units. A is $PT_2P_4T_4P_8$, B is PT_2P_4, C is PT_2, D is TP_3, E is TP_3T_3, and F is $TP_3T_3P_6$.

For each cluster model, a computational conformer search was performed. In line with experimental diffraction data suggesting that the P1M polymer is a sheet-like material[5] and chemical intuition, these searches generally found the lowest energy conformers of the cluster models to be flat 2D structures. The only noticeable exceptions are clusters containing small rings (e.g., rings with four triazine units, see later).

Focusing initially on the dendrimer-like structures, Figure 8 shows their calculated absorption spectra, while Figure 9 shows the trend for the energy of the lowest singlet excited state as a function of the number of triazine units in the oligomer. From Figure 9, it is clear that the energy of the lowest singlet excited state decreases steadily with increasing number of triazine units until it stabilizes after four to six triazine units. This steady convergence with oligomer size is advantageous from a modeling point of view because it makes the larger oligomers studied here suitable cluster models of the extended layers likely to be present in CTFs.

Figure 8 shows that the absorption spectra display a similar red shift as the lowest singlet excitation energies, although less clear-cut due to differences in peak intensity between the clusters. The spectra of oligomers with more triazine units are red-shifted (i.e., display peaks at longer wavelength) than oligomers with fewer triazine units. Peaks with significant intensity generally lie at slightly higher energy (shorter wavelength) than the lowest singlet excitation energy values shown in Figure 9. This observation finds it origin in the fact that just as for TP_3, the lowest energy excitations in the dendrimer-like clusters have

dx.doi.org/10.1021/jp411854f | J. Phys. Chem. C 2014, 118, 4314−4324

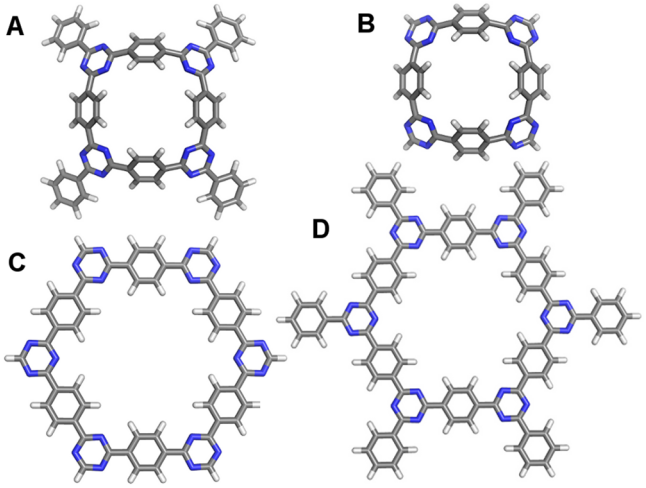

Figure 7. Ring models of the 1,4-Dicyanobenzene CTF.[5] For these ring systems (R) the nomenclature indicates the number of triazine units present in the structure (4 or 6) and the type of termination of the system (s signifies small, and these systems do not have terminal phenyl groups). A is R4, B is R4s, C is R6s, and D is R6.

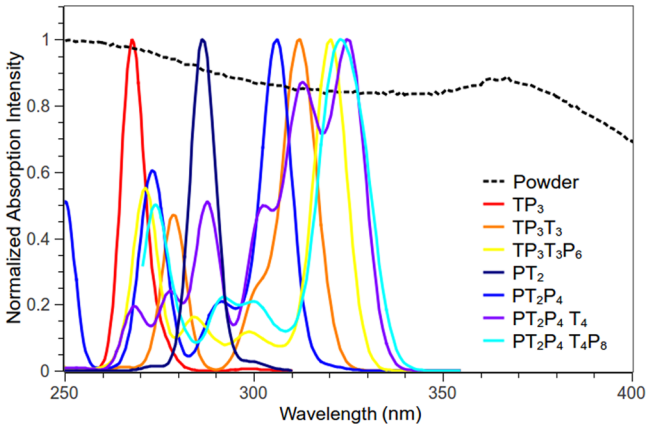

Figure 8. Experimental spectrum of P1M polymer[5] powder (black interrupted line) and TD-B3LYP/DZP predicted spectra of oligomers.

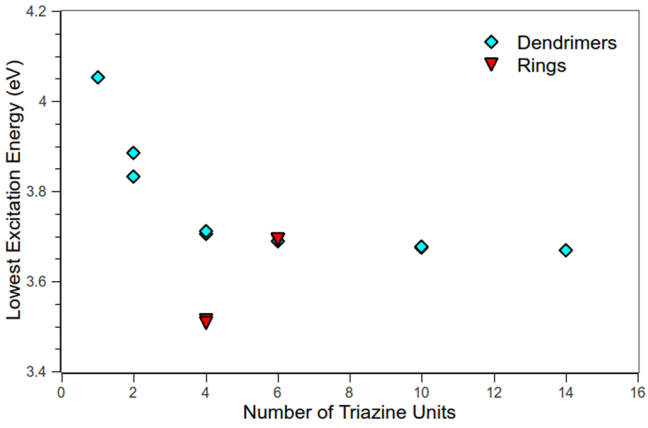

Figure 9. Trend in the TD-B3LYP/DZP predicted lowest excitation energies of the different oligomers as a function of the number of triazine units present.

n → π^* character and the $\pi \rightarrow \pi^*$ strong(er) intensity only appears at slightly higher energy. On the basis of these results, one can extrapolate that TD-B3LYP predicts that the absorption spectrum of an "infinite" isolated (i.e., nonstacked) dendrimer-like cluster is not expected to have absorption peaks at wavelengths larger than ~340 nm.

Clusters containing six-membered rings, where the six stands for the number of triazine units in the ring, arise naturally from extending the dendrimer-like clusters. The lowest energy conformations of such six-membered ring containing clusters are perfectly flat and show no sign of any ring strain. Figure 10

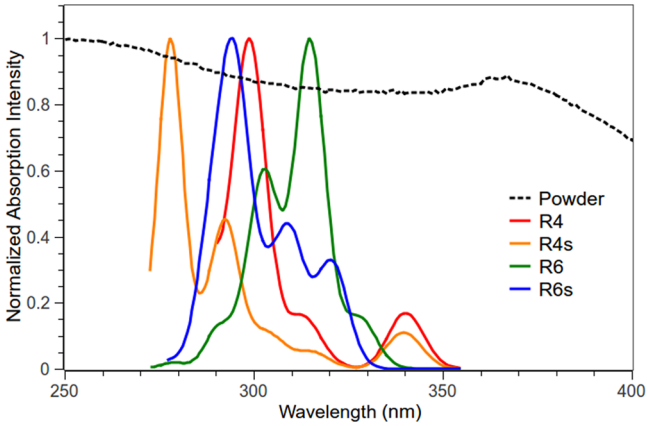

Figure 10. Experimental spectrum of P1M polymer[5] powder (black interrupted line) and theoretical spectra of ring oligomers calculated using TD-B3LYP/DZP.

shows the calculated absorption spectrum for the ring-cluster models and demonstrates that flat six-membered ring containing clusters behave essentially the same as the dendrimer-like clusters, without rings. The lowest singlet excitation of the six-membered ring is also extremely similar to that of the larger dendrimer-like clusters. (See Figure 9.) Higher energy conformers of six-membered ring containing clusters and clusters based on smaller rings (e.g., four-membered rings), however, are not flat and have spectra (and lowest singlet excitation energies) that are red-shifted relative to the dendrimer-like clusters. (See Figures 9 and 10.) Specifically, these structures differ from the flat structures by the fact that they have nonzero torsion angles between the adjacent benzene and triazine units (e.g., 16° on the inside and 19° on the outside of the lowest energy conformer of the four-membered ring). Naively, one might have assumed that increasing these torsion angles should lead to a blue shift instead of a red shift, as larger torsion angles should decrease the overlap between the π systems on adjacent units of the polymer. The exact physical origin of the red shift is thus unclear, but it is not due to a change in the electronic character of the excited states. The lowest states of the ring still have n → π^* character.

Having studied isolated oligomers, we next considered stacked structures. Dendrimer-like and ring-based clusters were stacked with the experimentally reported interlayer distance of 3.4 Å for the 1,4-dicyanobenzene CTF[2] (compared with 3.9 Å for TP_3), and their absorption spectra were calculated with TD-B3LYP. Stacking of the oligomers results just as in the case of TP_3 in a blue shift of the strong intensity peaks of the isolated oligomer and the appearance of new red-shifted peaks in the 320−400 nm spectral range where the isolated oligomers do not absorb light. Examples of this can be seen in Figures 11 and 13, which present TD-B3LYP predicted absorption spectra of PT_2 and TP_3T_3 stacks (illustration of some of the PT_2 stacking structures in Figure 12) and in the

dx.doi.org/10.1021/jp411854f | J. Phys. Chem. C 2014, 118, 4314−4324

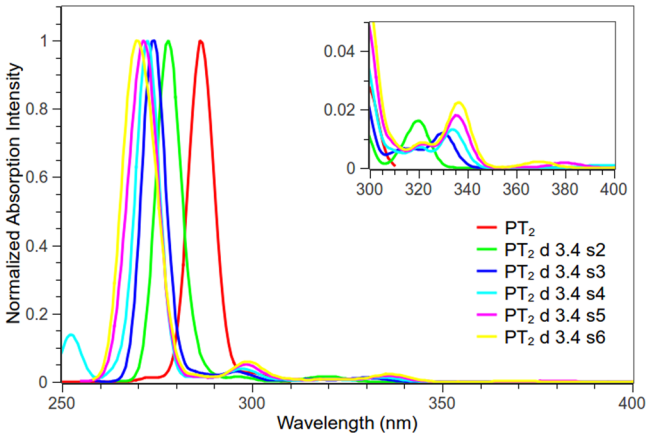

Figure 11. TD-B3LYP/DZP predicted spectra for a series of stacked PT_2 molecules. From a single molecule of PT_2 (red) up to a stacked system consisting of six PT_2 molecules. The distance between the molecules is constant at 3.4 Å. The insert shows a zoom-in of the spectra between 300 and 400 nm, where stacking results in the appearance of new red-shifted peaks. (See Figure S4 in section ESI-4 of the Supporting Information for a version with the experimental P1M spectrum.)

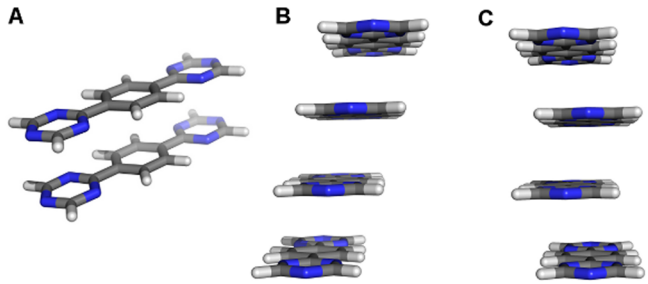

Figure 12. Illustrations of on-top stacking (A), four PT_2 molecules stacked with a consecutive shift of 1 Å (B), and four PT_2 molecules stack with an alternate shift of 1 Å (C).

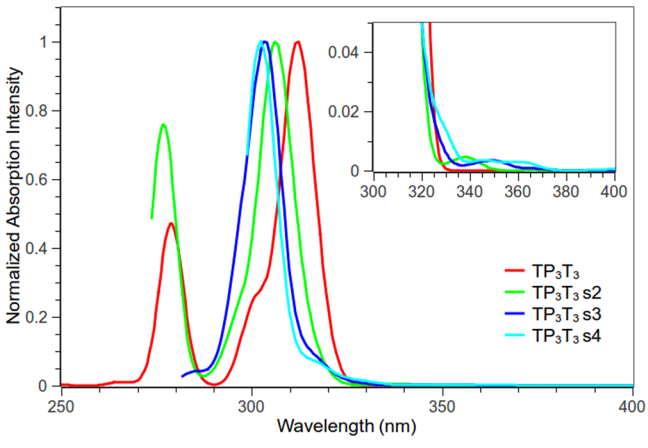

Figure 13. TD-B3LYP/DZP predicted spectra for a series of stacked TP_3T_3 molecules. From a single TP_3T_3 (red) up to a stacked system consisting of four TP_3T_3 molecules. The distance between the molecules is constant at 3.4 Å. The insert shows a zoom-in of the spectra between 300 and 400 nm, where stacking results in the appearance of new red-shifted peaks. (See Figure S5 in section ESI-4 of the Supporting Information for a version with the experimental P1M spectrum.)

ESI (Figures S6 and S7 in section ESI-4 of the Supporting Information) for the case of stacked $PT_2P_4T_4$ and two stacked six-rings. A comparison of the CC2/def2-SV(P) calculated spectra for isolated PT_2 and a two-stack (see Figure S9 in the section ESI-4 of the Supporting Information) yields results similar to those obtained with TD-B3LYP.

For all systems studied the blue shift of the main peak and the red shift of the new long-wavelength peaks rapidly converges with the numbers of layers stacked. The intensity of the red-shifted peaks relative to the blue-shifted main peaks, however, appears to grow constituently with every layer added, although from a low starting point for the larger oligomers. (See inserts of Figures 11 and 13 and Figures S6 and S7 in the Supporting Information.) Only calculations on stacks with a small number of layers (2−6, depending on the size of the isolated oligomer) are computationally tractable, but extrapolating the observed trend in relative intensities to the numbers of layers a stack might have in actual samples (∼100−1000) suggests that for such samples the red-shifted peaks will be of similar intensity to the blue-shifted peak. Just as for TP_3, stacking in the case of oligomers is thus expected to lead to the type of two-peak spectrum observed experimentally for P1 and P1M. Moreover, in line with experiment, the overall spectra of the oligomers are predicted to be red-shifted compared with that of stacked TP_3. Selected examples for PT_2, finally, also suggest that stacking arrangements in which subsequent layers are shifted relative to another have slightly larger red shifts than simple on-top stacking. (See Figure 11 and Figure S3 in section ESI-4 of the Supporting Information.)

The lowest excited state of the oligomers is always dark, that is, without oscillator strength, either inherently on symmetry grounds or accidentally in practice. In the latter case, the oscillator strength decreases strongly with the number of layers stacked and the excitation lifetimes reach values of seconds or larger. It is tantalizing to explain these red and blue shifts in terms of Kasha's exciton model,[45] with excited states on isolated molecules coupled only electrostatically, or in terms of Kazmaier and Hoffmann's crystallochromy model,[47] where the HOMO and LUMO responsible for the excited states split and form bands upon stacking. However, visualization of the involved orbitals (see Figures S10 and S11 in the Supporting Information for a stack of four PT_2 molecules) appears to show strong mixing of the empty orbitals on the different oligomers, resulting in these orbitals (e.g., the lowest unoccupied molecular orbital) to be delocalized over multiple or even all stacked layers. Hence, one should be careful with overinterpreting models that treat the excited states of stacks in a basis of the unperturbed molecular excited states or the orbitals that underlie them.

In a next step, we calculated the fluorescence spectra of the smaller dendrimer-like and ring-based clusters. Just as for TP_3, we optimized the lowest excited state of the cluster models. Table 3 gives the obtained fluorescence energies for the different cluster models. In the case of the ring-based clusters, we find two fundamentally different types of minima: one type of minimum where the distortion is delocalized over all triazine units in the ring and one type of minimum where all distortion is localized in just one triazine unit. The localized ring minima always lie lower in S_1 total energy and have the smaller fluorescence energy. In the case of the dendrimer-like clusters, only localized type minima were obtained. See Figure S12 in section ESI-5 of the Supporting Information for an illustration of the structural changes associated with the localized minimum in the case of PT_2.

dx.doi.org/10.1021/jp411854f | J. Phys. Chem. C 2014, 118, 4314−4324

Table 3. Fluorescence Energies (Fl) of Different Oligomers Calculated using TD-B3LYP/DZP

structure	Fl energy (eV)	Fl wavelength (nm)
TP_3	2.67	465
PT_2	2.22	559
TP_3T_3	2.42	513
PT_2P_4	2.41	515
R4	3.33/2.36	372/525
R4s	3.32/2.28	373/545
R6	3.59/2.43	345/510
R6s	3.60/2.35	344/528

As can be seen in Table 3, the fluorescence energies predicted for both the dendrimer-like cluster and ring-based cluster (localized minima) fit well with the experimentally measured P1M fluorescence spectrum. However, all dendrimer-like clusters inherit the TP_3 issue of extremely low oscillator strengths and long excited-state lifetimes at the S_1 minimum energy geometry (~0.03−30 s), effectively ruling them out as the chromophores responsible for the fluorescence. Moreover, as previously discussed, the lowest excited state at the ground-state geometry of a stack of oligomers is generally dark, and hence the mere fact of stacking oligomers is unlikely to change this observation. The localized minima in the rings have in contrast relatively short excited-state lifetimes (e.g., 2 and 79 microseconds for the lowest energy conformer of the four-membered and six-membered rings, respectively) and hence make suitable fluorescence chromophores, where furthermore the lifetime appears to decrease and hence likeliness of fluorescence increases with the "strain" of chromophore (e.g., when going from a six-membered to a four-membered ring). The lack of fluorescence in TP_3 has been explained in the past by the $n \rightarrow \pi^*$ character of the lowest excitation.[40,41] The five orders of magnitude reduction in predicted excited-state lifetime in the case of rings, however, does not appear to stem from a change in electronic character of S_1 in its minimum energy geometry, as that is still $n \rightarrow \pi^*$.

Rings are thus the likely chromophores responsible for fluorescence in 1,4-dicyanobenzene CTF materials, such as P1M. Excited-state total-energy considerations further suggest, just as previous observed in the case of pyrene,[17,18] that it is energetically favorable for the excited state to move from less strained to more strained parts of the framework (i.e., for the process six-membered ring* + four-membered ring → six-membered ring + four-membered ring* to be exothermic, where the asterisk indicates the chromophore on which the excited state is localized). More strained rings, such as four-membered rings, if present as "defects" in the 1,4-dicyanobenzene CTF materials, are thus especially likely to contribute to the experimentally observed fluorescence signal as (i) they have a shorter excited state lifetime and hence are more likely to display stronger fluorescence and (ii) there is an energetic driving force for the excited state to move to these strained chromophores. It would be interesting to characterize CTFs in future work using time-resolved fluorescence spectroscopy and measure their fluorescence lifetime experimentally. The presence of defects, or more generally the presence of multiple fluorescence chromophores, might then show up as a multimodal fluorescence lifetime distribution for a given CTF.

Finally, it is interesting to reflect on the differences in the spectra reported in our previous work[5] for the 1,4-dicyanobenzene CTF synthesized with microwave (P1M) and conventional heating (P1). The top of the first absorption peak in P1 is red-shifted by ~10 nm relative to that of P1M (see Figure 5), while the fluorescence spectra of both materials are very similar. The absorption red shift is small enough to be an experimental artifact or find its origin in the natural synthetic variation between different batches. However, because this red shift appears similar to the red shift found in our calculations for non-on-top stacking arrangements (i.e., stacking with shifts or slides between layers) and because P1M is reported to show X-ray diffraction consistent with on-top stacking of hexagonal layers while P1 is X-ray amorphous, another interpretation might be that this red shift arises from stacking disorder in P1. The similarity of the P1 and P1M fluorescence spectra is inline with our assessment that this fluorescence originates from a localized center and hence is less sensitive to the exact stacking arrangement.

CONCLUSIONS

It is demonstrated that the optical absorption and fluorescence spectra of triazine CTFs can be most likely understood in terms of stacked flat layers based on rings. The stacking is shown to lead to the appearance of new red-shifted peaks in the absorption spectrum, absent in isolated layers and the blue shift of existing peaks, resulting in the characteristic two-peak absorption spectrum observed experimentally. Rings (in particular, if present, the more strained small rings) are the likely sources of fluorescence in CTFs because the excited-state lifetime in oligomers without rings is predicted to be so long that any fluorescence will be extremely weak and non-competitive with dark de-excitation pathways. Subtle differences between the experimental absorption spectra of CTFs prepared using different synthesis routes are shown to possibly find their origin in the different relative arrangement of the stacked layers.

ASSOCIATED CONTENT

Supporting Information

Additional CC2 and TD-B3LYP spectra and figures of stacked structures, a discussion about range-separated density functionals and stacked systems, and tables with the lowest excitation energies for various systems can be found in the Supporting Information. This material is available free of charge via the Internet at http://pubs.acs.org.

AUTHOR INFORMATION

Corresponding Authors

*D.J.A.: E-mail: d.j.adams@liverpool.ac.uk.
*M.A.Z.: E-mail: m.zwijnenburg@ucl.ac.uk.

Notes

The authors declare no competing financial interest.

ACKNOWLEDGMENTS

Dr. Michael Bojdys and Dr. Shijie Ren are kindly acknowledged for useful discussion. M.A.Z. thanks the U.K. Engineering and Physical Sciences Research Council (EPSRC) for a Career Acceleration Fellowship (Grant EP/I004424/1). Computational time on HECToR the U.K.'s national high-performance computing service (via our membership of the U.K.'s HPC Materials Chemistry Consortium, which is funded by EPSRC grants EP/F067496/1 and EP/L000202/1) and the EPSRC U.K. National Service for Computational Chemistry Software (NSCCS) at Imperial College London is gratefully acknowledged.

We thank the EPSRC for funding (EP/H000925/1). A.I.C. is a Royal Society Wolfson award holder.

REFERENCES

(1) Kuhn, P.; Thomas, A.; Antonietti, M. Toward Tailorable Porous Organic Polymer Networks: A High-Temperature Dynamic Polymerization Scheme Based on Aromatic Nitriles. *Macromolecules* **2008**, *42*, 319−326.
(2) Kuhn, P.; Antonietti, M.; Thomas, A. Porous, Covalent Triazine-Based Frameworks Prepared by Ionothermal Synthesis. *Angew. Chem., Int. Ed.* **2008**, *47*, 3450−3453.
(3) Kuhn, P.; Forget, A. l.; Su, D.; Thomas, A.; Antonietti, M. From Microporous Regular Frameworks to Mesoporous Materials with Ultrahigh Surface Area: Dynamic Reorganization of Porous Polymer Networks. *J. Am. Chem. Soc.* **2008**, *130*, 13333−13337.
(4) Bojdys, M. J.; Jeromenok, J.; Thomas, A.; Antonietti, M. Rational Extension of the Family of Layered, Covalent, Triazine-Based Frameworks with Regular Porosity. *Adv. Mater.* **2010**, *22*, 2202−2205.
(5) Ren, S.; Bojdys, M. J.; Dawson, R.; Laybourn, A.; Khimyak, Y. Z.; Adams, D. J.; Cooper, A. I. Porous, Fluorescent, Covalent Triazine-Based Frameworks Via Room-Temperature and Microwave-Assisted Synthesis. *Adv. Mater.* **2012**, *24*, 2357−2361.
(6) Ren, S.; Dawson, R.; Laybourn, A.; Jiang, J.-x.; Khimyak, Y.; Adams, D. J.; Cooper, A. I. Functional Conjugated Microporous Polymers: From 1,3,5-Benzene to 1,3,5-Triazine. *Polym. Chem.* **2012**, *3*, 928−934.
(7) Katekomol, P.; Roeser, J.; Bojdys, M.; Weber, J.; Thomas, A. Covalent Triazine Frameworks Prepared from 1,3,5-Tricyanobenzene. *Chem. Mater.* **2013**, *25*, 1542−1548.
(8) Wang, X.; Maeda, K.; Chen, X.; Takanabe, K.; Domen, K.; Hou, Y.; Fu, X.; Antonietti, M. Polymer Semiconductors for Artificial Photosynthesis: Hydrogen Evolution by Mesoporous Graphitic Carbon Nitride with Visible Light. *J. Am. Chem. Soc.* **2009**, *131*, 1680−1681.
(9) Zhang, J.; Chen, X.; Takanabe, K.; Maeda, K.; Domen, K.; Epping, J. D.; Fu, X.; Antonietti, M.; Wang, X. Synthesis of a Carbon Nitride Structure for Visible-Light Catalysis by Copolymerization. *Angew. Chem., Int. Ed.* **2010**, *49*, 441−444.
(10) Schwinghammer, K.; Tuffy, B.; Mesch, M. B.; Wirnhier, E.; Martineau, C.; Taulelle, F.; Schnick, W.; Senker, J.; Lotsch, B. V. Triazine-Based Carbon Nitrides for Visible-Light-Driven Hydrogen Evolution. *Angew. Chem., Int. Ed.* **2013**, *52*, 2435−2439.
(11) Cooper, A. I. Conjugated Microporous Polymers. *Adv. Mater.* **2009**, *21*, 1291−1295.
(12) Dawson, R.; Laybourn, A.; Khimyak, Y. Z.; Adams, D. J.; Cooper, A. I. High Surface Area Conjugated Microporous Polymers: The Importance of Reaction Solvent Choice. *Macromolecules* **2010**, *43*, 8524−8530.
(13) Dawson, R.; Cooper, A. I.; Adams, D. J. Nanoporous Organic Polymer Networks. *Prog. Polym. Sci.* **2012**, *37*, 530−563.
(14) Roeser, J.; Kailasam, K.; Thomas, A. Covalent Triazine Frameworks as Heterogeneous Catalysts for the Synthesis of Cyclic and Linear Carbonates from Carbon Dioxide and Epoxides. *ChemSusChem* **2012**, *5*, 1793−1799.
(15) Zhang, W.; Li, C.; Yuan, Y.-P.; Qiu, L.-G.; Xie, A.-J.; Shen, Y.-H.; Zhu, J.-F. Highly Energy-and Time-Efficient Synthesis of Porous Triazine-Based Framework: Microwave-Enhanced Ionothermal Polymerization and Hydrogen Uptake. *J. Mater. Chem.* **2010**, *20*, 6413−6415.
(16) Blanc, F.; Chong, S. Y.; McDonald, T. O.; Adams, D. J.; Pawsey, S.; Caporini, M. A.; Cooper, A. I. Dynamic Nuclear Polarization NMR Spectroscopy Allows High-Throughput Characterization of Microporous Organic Polymers. *J. Am. Chem. Soc.* **2013**, *135*, 15290−15293.
(17) Zwijnenburg, M. A. Elucidating the Microscopic Origin of the Unique Optical Properties of Polypyrene. *J. Phys. Chem. C* **2012**, *116*, 20191−20198.
(18) Zwijnenburg, M. A.; Cheng, G.; McDonald, T. O.; Jelfs, K. E.; Jiang, J.-X.; Ren, S.; Hasell, T.; Blanc, F.; Cooper, A. I.; Adams, D. J. Shedding Light on Structure−Property Relationships for Conjugated Microporous Polymers: The Importance of Rings and Strain. *Macromolecules* **2013**, *46*, 7696−7704.
(19) Wang, J.; Xu, F.; Cai, T.; Shen, Q. Addition of Amines to Nitriles Catalyzed by Ytterbium Amides: An Efficient One-Step Synthesis of Monosubstituted N-Arylamidines. *Org. Lett.* **2008**, *10*, 445−448.
(20) Schaefer, F. C.; Peters, G. A. Synthesis of the S-Triazine System. Iii. 1 Trimerization of Imidates. *J. Org. Chem.* **1961**, *26*, 2778−2784.
(21) Furche, F.; Ahlrichs, R. Erratum: "Time-Dependent Density Functional Methods for Excited State Properties" [J. Chem. Phys. **117**, 7433 (2002)]. *J. Phys. Chem.* **2004**, *121*, 12772.
(22) Furche, F.; Ahlrichs, R. Adiabatic Time-Dependent Density Functional Methods for Excited State Properties. *J. Phys. Chem.* **2002**, *117*, 7433−7447.
(23) Christiansen, O.; Koch, H.; Jørgensen, P. The Second-Order Approximate Coupled Cluster Singles and Doubles Model Cc2. *Chem. Phys. Lett.* **1995**, *243*, 409−418.
(24) Jorgensen, W. L.; Tirado-Rives, J. Potential Energy Functions for Atomic-Level Simulations of Water and Organic and Biomolecular Systems. *Proc. Natl. Acad. Sci. U.S.A.* **2005**, *102*, 6665−6670.
(25) Kolossváry, I.; Guida, W. C. Low Mode Search. An Efficient, Automated Computational Method for Conformational Analysis: Application to Cyclic and Acyclic Alkanes and Cyclic Peptides. *J. Am. Chem. Soc.* **1996**, *118*, 5011−5019.
(26) *Macromodel*, version 9.9; Schrödinger, LLC: New York, 2012.
(27) Becke, A. D. Density-Functional Thermochemistry. Iii. The Role of Exact Exchange. *J. Phys. Chem.* **1993**, *98*, 5648−5652.
(28) Yanai, T.; Tew, D. P.; Handy, N. C. A New Hybrid Exchange−Correlation Functional Using the Coulomb-Attenuating Method (Cam-B3lyp). *Chem. Phys. Lett.* **2004**, *393*, 51−57.
(29) Hirata, S.; Head-Gordon, M. Time-Dependent Density Functional Theory within the Tamm−Dancoff Approximation. *Chem. Phys. Lett.* **1999**, *314*, 291−299.
(30) Peach, M. J. G.; Williamson, M. J.; Tozer, D. J. Influence of Triplet Instabilities in Tddft. *J. Chem. Theory Comput.* **2011**, *7*, 3578−3585.
(31) Schäfer, A.; Horn, H.; Ahlrichs, R. Fully Optimized Contracted Gaussian Basis Sets for Atoms Li to Kr. *J. Phys. Chem.* **1992**, *97*, 2571−2577.
(32) Hehre, W. J.; Ditchfield, R.; Pople, J. A. Self—Consistent Molecular Orbital Methods. Xii. Further Extensions of Gaussian—Type Basis Sets for Use in Molecular Orbital Studies of Organic Molecules. *J. Phys. Chem.* **1972**, *56*, 2257−2261.
(33) Weigend, F.; Ahlrichs, R. Balanced Basis Sets of Split Valence, Triple Zeta Valence and Quadruple Zeta Valence Quality for H to Rn: Design and Assessment of Accuracy. *Phys. Chem. Chem. Phys.* **2005**, *7*, 3297−3305.
(34) Klamt, A.; Schuurmann, G. Cosmo: A New Approach to Dielectric Screening in Solvents with Explicit Expressions for the Screening Energy and Its Gradient. *J. Chem. Soc.* **1993**, 799−805.
(35) Schäfer, A.; Klamt, A.; Sattel, D.; Lohrenz, J. C.; Eckert, F. Cosmo Implementation in Turbomole: Extension of an Efficient Quantum Chemical Code Towards Liquid Systems. *Phys. Chem. Chem. Phys.* **2000**, *2*, 2187−2193.
(36) Ahlrichs, R.; Haser, M.; Kolmel, C.; Horn, H.; Baer, M. Turbomole, University of Karlsruhe, 1988;(B) M. Hiker and R. Ahlrichs. *J. Comput. Chem.* **1989**, *10*, 104.
(37) van Wüllen, C. Shared-Memory Parallelization of the Turbomole Programs Aoforce, Escf, and Egrad: How to Quickly Parallelize Legacy Code. *J. Comput. Chem.* **2011**, *32*, 1195−1201.
(38) Valiev, M.; Bylaska, E. J.; Govind, N.; Kowalski, K.; Straatsma, T. P.; Van Dam, H. J. J.; Wang, D.; Nieplocha, J.; Apra, E.; Windus, T. L.; et al. Nwchem: A Comprehensive and Scalable Open-Source Solution for Large Scale Molecular Simulations. *Comput. Phys. Commun.* **2010**, *181*, 1477−1489.
(39) Schmidt, M. W.; Baldridge, K. K.; Boatz, J. A.; Elbert, S. T.; Gordon, M. S.; Jensen, J. H.; Koseki, S.; Matsunaga, N.; Nguyen, K. A.; Su, S.; et al. General Atomic and Molecular Electronic Structure System. *J. Comput. Chem.* **1993**, *14*, 1347−1363.

(40) Chen, A. C. A.; Wallace, J. U.; Wei, S. K. H.; Zeng, L.; Chen, S. H.; Blanton, T. N. Light-Emitting Organic Materials with Variable Charge Injection and Transport Properties. *Chem. Mater.* **2006**, *18*, 204−213.
(41) Zhong, H.; Xu, E.; Zeng, D.; Du, J.; Sun, J.; Ren, S.; Jiang, B.; Fang, Q. New Optoelectronic Materials Based on Bitriazines: Synthesis and Properties. *Org. Lett.* **2008**, *10*, 709−712.
(42) Lindeman, S. V.; Shklover, V. E.; Struchkov, Y. T.; Mitina, L. M.; Pankratov, V. A. Refinement of the Structure of Sym-Triphenyltriazine. *J. Struct. Chem.* **1984**, *25*, 162−164.
(43) Scheibe, G. Über Die Veränderlichkeit Der Absorptionsspektren in Lösungen Und Die Nebenvalenzen Als Ihre Ursache. *Angew. Chem.* **1937**, *50*, 212−219.
(44) Jelley, E. E. Spectral Absorption and Fluorescence of Dyes in the Molecular State. *Nature* **1936**, *138*, 1009−1010.
(45) Kasha, M.; Rawls, H.; El-Bayoumi, M. A. The Exciton Model in Molecular Spectroscopy. *Pure Appl. Chem.* **1965**, *11*, 371−392.
(46) Saikin, S. K.; Eisfeld, A.; Valleau, S.; Aspuru-Guzik, A. Photonics Meets Excitonics: Natural and Artificial Molecular Aggregates. *Nanophotonics* **2013**, *2*, 21−38.
(47) Kazmaier, P. M.; Hoffmann, R. A Theoretical Study of Crystallochromy. Quantum Interference Effects in the Spectra of Perylene Pigments. *J. Am. Chem. Soc.* **1994**, *116*, 9684−9691.